ISSN 2220-3206 (online)

World Journal of *Psychiatry*

World J Psychiatry 2024 April 19; 14(4): 489-599

Published by Baishideng Publishing Group Inc

WJP World Journal of Psychiatry

Contents

Monthly Volume 14 Number 4 April 19, 2024

EDITORIAL

REVIEW

ORIGINAL ARTICLE

Case Control Study

Retrospective Cohort Study

Retrospective Study

Observational Study

World Journal of Psychiatry

Monthly Volume 14 Number 4 April 19, 2024

Contents

World Journal of Psychiatry

Monthly Volume 14 Number 4 April 19, 2024

Contents

ABOUT COVER

Editorial Board Member of *World Journal of Psychiatry*, Sujita Kumar Kar, MD, Additional Professor, Department of Psychiatry, King George's Medical University, Lucknow-226003, UP, India. drsujita@gmail.com

AIMS AND SCOPE

The primary aim of *World Journal of Psychiatry* (*WJP*, *World J Psychiatry*) is to provide scholars and readers from various fields of psychiatry with a platform to publish high-quality basic and clinical research articles and communicate their research findings online.

WJP mainly publishes articles reporting research results and findings obtained in the field of psychiatry and covering a wide range of topics including adolescent psychiatry, biological psychiatry, child psychiatry, community psychiatry, ethnopsychology, psychoanalysis, psychosomatic medicine, *etc*.

INDEXING/ABSTRACTING

The *WJP* is now abstracted and indexed in Science Citation Index Expanded (SCIE, also known as SciSearch®), Current Contents/Clinical Medicine, Journal Citation Reports/Science Edition, PubMed, PubMed Central, Reference Citation Analysis, China Science and Technology Journal Database, and Superstar Journals Database. The 2023 Edition of Journal Citation Reports® cites the 2022 impact factor (IF) for *WJP* as 3.1; IF without journal self cites: 2.9; 5-year IF: 4.2; Journal Citation Indicator: 0.52; Ranking: 91 among 155 journals in psychiatry; and Quartile category: Q3.

RESPONSIBLE EDITORS FOR THIS ISSUE

Production Editor: *Si Zhao*; **Production Department Director:** *Xu Guo*; **Cover Editor:** *Jia-Ping Yan*.

NAME OF JOURNAL
World Journal of Psychiatry

ISSN
ISSN 2220-3206 (online)

LAUNCH DATE
December 31, 2011

FREQUENCY
Monthly

EDITORS-IN-CHIEF
Ting-Shao Zhu

EDITORIAL BOARD MEMBERS
https://www.wjgnet.com/2220-3206/editorialboard.htm

PUBLICATION DATE
April 19, 2024

INSTRUCTIONS TO AUTHORS
https://www.wjgnet.com/bpg/gerinfo/204

GUIDELINES FOR ETHICS DOCUMENTS
https://www.wjgnet.com/bpg/GerInfo/287

GUIDELINES FOR NON-NATIVE SPEAKERS OF ENGLISH
https://www.wjgnet.com/bpg/gerinfo/240

PUBLICATION ETHICS
https://www.wjgnet.com/bpg/GerInfo/288

PUBLICATION MISCONDUCT
https://www.wjgnet.com/bpg/gerinfo/208

ARTICLE PROCESSING CHARGE
https://www.wjgnet.com/bpg/gerinfo/242

STEPS FOR SUBMITTING MANUSCRIPTS
https://www.wjgnet.com/bpg/GerInfo/239

ONLINE SUBMISSION
https://www.f6publishing.com

World Journal of Psychiatry

Submit a Manuscript: https://www.f6publishing.com

World J Psychiatry 2024 April 19; 14(4): 563-581

DOI: 10.5498/wjp.v14.i4.563

ISSN 2220-3206 (online)

ORIGINAL ARTICLE

Basic Study

Tanshinone IIA improves Alzheimer's disease *via* RNA nuclear-enriched abundant transcript 1/microRNA-291a-3p/member RAS oncogene family Rab22a axis

Long-Xiu Yang, Man Luo, Sheng-Yu Li

Specialty type: Psychiatry

Provenance and peer review: Unsolicited article; Externally peer reviewed.

Peer-review model: Single blind

Peer-review report's scientific quality classification

Grade A (Excellent): 0
Grade B (Very good): 0
Grade C (Good): C, C
Grade D (Fair): 0
Grade E (Poor): 0

P-Reviewer: Jeong KY, South Korea

Received: October 11, 2023
Peer-review started: October 11, 2023
First decision: December 26, 2023
Revised: January 9, 2024
Accepted: February 28, 2024
Article in press: February 28, 2024
Published online: April 19, 2024

Long-Xiu Yang, Man Luo, Sheng-Yu Li, Department of Neurology, The First Affiliated Hospital of Guangxi Medical University, Nanning 530000, Guangxi Zhuang Autonomous Region, China

Sheng-Yu Li, Department of Neurology, Wuming Hospital of Guangxi Medical University, Nanning 530199, Guangxi Zhuang Autonomous Region, China

Corresponding author: Sheng-Yu Li, MD, Doctor, Teacher, Department of Neurology, The First Affiliated Hospital of Guangxi Medical University, No. 6 Shuangyong Road, Qingxiu District, Nanning 530000, Guangxi Zhuang Autonomous Region, China. 15177821212@163.com

Abstract

BACKGROUND

Alzheimer's disease (AD) is a neurodegenerative condition characterized by oxidative stress and neuroinflammation. Tanshinone IIA (Tan-IIA), a bioactive compound isolated from *Salvia miltiorrhiza* plants, has shown potential neuroprotective effects; however, the mechanisms underlying such a function remain unclear.

AIM

To investigate potential Tan-IIA neuroprotective effects in AD and to elucidate their underlying mechanisms.

METHODS

Hematoxylin and eosin staining was utilized to analyze structural brain tissue morphology. To assess changes in oxidative stress and neuroinflammation, we performed enzyme-linked immunosorbent assay and western blotting. Additionally, the effect of Tan-IIA on AD cell models was evaluated *in vitro* using the 3-(4,5-dimethylthiazol-2-yl)-2,5-diphenyltetrazolium bromide assay. Genetic changes related to the long non-coding RNA (lncRNA) nuclear-enriched abundant transcript 1 (NEAT1)/microRNA (miRNA, miR)-291a-3p/member RAS oncogene family Rab22a axis were assessed through reverse transcription quantitative polymerase chain reaction.

RESULTS

In vivo, Tan-IIA treatment improved neuronal morphology and attenuated oxidative stress and neuroinflammation in the brain tissue of AD mice. *In vitro*

experiments showed that Tan-IIA dose-dependently ameliorated the amyloid-beta 1-42-induced reduction of neural stem cell viability, apoptosis, oxidative stress, and neuroinflammation. In this process, the lncRNA NEAT1 - a potential therapeutic target - is highly expressed in AD mice and downregulated *via* Tan-IIA treatment. Mechanistically, NEAT1 promotes the transcription and translation of Rab22a *via* miR-291a-3p, which activates nuclear factor kappa-B (NF-κB) signaling, leading to activation of the pro-apoptotic B-cell lymphoma 2-associated X protein and inhibition of the anti-apoptotic B-cell lymphoma 2 protein, which exacerbates AD. Tan-IIA intervention effectively blocked this process by inhibiting the NEAT1/miR-291a-3p/Rab22a axis and NF-κB signaling.

CONCLUSION

This study demonstrates that Tan-IIA exerts neuroprotective effects in AD by modulating the NEAT1/miR-291a-3p/Rab22a/NF-κB signaling pathway, serving as a foundation for the development of innovative approaches for AD therapy.

Key Words: Tanshinone IIA; Alzheimer's disease; Nuclear-enriched abundant transcript 1; Member of RAS oncogene family Rab22a; Reactive oxygen species

Core Tip: Tanshinone IIA (Tan-IIA), a compound isolated from *Salvia miltiorrhiza*, demonstrates neuroprotective effects against Alzheimer's disease (AD). This study reveals that Tan-IIA improves neuronal health, reduces oxidative stress and neuroinflammation, and promotes neural stem cell viability. Importantly, it targets the nuclear-enriched abundant transcript 1/microRNA-291a-3p/member RAS oncogene family Rab22a/nuclear factor kappa-B pathway, offering a potential therapeutic avenue for AD.

Citation: Yang LX, Luo M, Li SY. Tanshinone IIA improves Alzheimer's disease *via* RNA nuclear-enriched abundant transcript 1/microRNA-291a-3p/member RAS oncogene family Rab22a axis. *World J Psychiatry* 2024; 14(4): 563-581
URL: https://www.wjgnet.com/2220-3206/full/v14/i4/563.htm
DOI: https://dx.doi.org/10.5498/wjp.v14.i4.563

INTRODUCTION

Alzheimer's disease (AD), the most common cause of dementia worldwide, is a progressive neurological condition that affects millions of individuals and presents a serious public health issue[1,2]. The amyloid-beta 1-42 (Aβ1-42) peptide is a primary component of the amyloid plaques found in the brains of individuals with AD. It is believed to play a critical role in the neuropathology of AD by initiating a cascade of events that leads to neuronal dysfunction and death[3]. Memory loss and cognitive decline are caused by the buildup of Aβ plaques, neurofibrillary tangles, and synaptic and neuronal loss in individuals with AD[4-6]. Despite extensive research on AD, current treatment options only focus on symptomatic relief rather than disease remission, and the development of new therapeutic agents and targets is required to improve the disease prognosis.

Growing evidence points to neuroinflammation and oxidative stress being key factors in the etiology of AD[7,8]. Nitric oxide (NO) gas is produced in greater amounts when there is an excessive buildup of reactive oxygen species (ROS) in the body. An increased production of NO causes oxidative stress, which damages neurons and exacerbates AD[9]. This process lowers the levels of the antioxidants superoxide dismutase (SOD) and glutathione (GSH), making them less effective at scavenging ROS[10,11]. In addition, the release of neuroinflammatory factors, such as tumor necrosis factor-alpha (TNF-α), interleukin (IL)-1β, and IL-6, exacerbates neuronal damage and contributes to the progression of AD[12,13]. Long non-coding RNA (lncRNA) furthermore acts as a molecular sponge for microRNA (miR, miRNA) adsorption to regulate miRNA expression[14], and such changes in miRNA expression critically affect the transcription and translation of downstream targets[15]. For example, a study by Zhao *et al*[16] showed that the lncRNA nuclear-enriched abundant transcript 1 (NEAT1) promotes the development of AD through the miR-124/beta-site amyloid precursor protein-cleaving enzyme axis. In addition, miR-291a-3p, which is associated with inflammation, oxidative stress, and apoptosis, may be downregulated in neural injury[17,18]; however, its role and mechanism of function in AD remain unclear.

RAB22A, member RAS oncogene family (Rab22a) is another important tumor regulator[19,20], but its mechanism of action in AD is unclear. Its role in promoting neuroinflammation and oxidative stress[21] warrants the inclusion of Rab22a in the present study to explore its role in AD, especially since it affects Aβ accumulation[22]. Additionally, the nuclear factor kappa-B (NF-κB) pathway is triggered by the neuroinflammatory response in AD, which can aggravate the disease progression. The role of the B-cell lymphoma 2 (Bcl-2) protein in this process is significantly inhibited in contrast to that of pro-apoptotic proteins; the greater the ratio of Bcl-2/Bcl-2-associated X protein (Bax), the greater the anti-apoptotic ability. However, the role of Rab22a on NF-κB and the regulation of downstream pro- and anti-apoptotic proteins require elucidation.

Salvia miltiorrhiza, also known as danshen or red sage, produces a bioactive molecule called tanshinone IIA (Tan-IIA; chemical structure depicted in Figure 1A) with reportedly anti-inflammatory, antioxidant, and anti-apoptotic activities [23,24]. Previous studies demonstrated that Tan-IIA reduces oxidative stress and neuroinflammation, two factors known to worsen AD[25,26]. Although Tan-IIA has been shown to improve AD, the mechanism underlying this improvement is not well understood.

In this study, we investigate processes involving the NEAT1/miR-291a-3p/Rab22a/NF-κB signaling pathway that may underlie the neuroprotective benefits of Tan-IIA, using both *in vivo* and *in vitro* models of AD. Our results help to clarify the intricate regulatory network that controls oxidative stress and neuroinflammation connected to AD and may serve as a foundation for the creation of new treatment options for the disease.

MATERIALS AND METHODS

Animal models and neural stem cell isolation

The Guangdong Medical Experimental Animal Center (Guangzhou, China) provided all mice; AD was induced in some mice *via* a bilateral injection of Aβ1-42 oligomers into the CA1 region of the hippocampus, as previously described[27]. All animal treatments were approved by the Guangxi Medical University's Animal Care and Use Committee [approval no. 2021(KY-E-292); Nanning, China] and were carried out in accordance with the Guide for the Care and Use of Laboratory Animals.

The mice were maintained under a 12-h light/dark cycle and provided with unlimited access to food and water. Mice were randomly placed in one of four treatment groups (n = 6 each): A control group, comprising healthy mice; an AD group, in which AD was induced without further treatment; and two Tan-IIA groups, with AD mice receiving either 5 or 20 mg/kg of Tan-IIA (HY-N0135; MedChemExpress LLC, NJ, United States). Tan-IIA was dissolved in dimethyl sulfoxide (DMSO; Solarbio, Beijing, China) and administered intraperitoneally once daily for 4 wk in mice of the relevant treatment groups. Subsequently, the mice were anesthetized and sacrificed, and their brain tissues were removed and placed in Hank's balanced salt solution (Gibco, Thermo Fisher Scientific, MA, United States) with 1% penicillin-streptomycin (Gibco) to isolate the neural stem cells (NSCs). Tissues from the hippocampus and subventricular zone were carefully removed, chopped, and subjected to enzymatic digestion with trypsin-EDTA (Gibco) for 15 min at 37 °C. Fetal bovine serum (Gibco) was used to terminate digestion, after which the cell solution was filtered through a 40 m mesh cell strainer (BD Biosciences, CA, United States) to remove debris. The cells were centrifuged at 300 rpm for 5 min, and the resulting cell pellet was resuspended and cultured in NSC culture medium (Procell, Wuhan, China) at 37 °C and in 5% CO_2. The medium was replaced every 2 d, and the NSCs were passaged until 80%-90% confluence was reached before being used for subsequent experiments.

Immunofluorescence analysis

The obtained NSCs were incubated with bovine serum albumin for 30 min and incubated further (overnight, at 4 °C and in the dark) with microtubule-associated protein 2 (MAP2; 1:500, ab254264; Abcam, Cambridge, United Kingdom), β III tubulin (3 μg/mL, ab18207; Abcam), and nuclear factor erythroid 2-related factor 2 (Nrf2; 1:100, ab62352; Abcam) antibodies. Thereafter, the cells were incubated at 37 °C for 1 h with either goat anti-rabbit Alexa Fluor® 488 (1:250, ab150077; Abcam) or 647-conjugated secondary antibodies. Finally, the NSCs were mounted on microscope slides using a gold antifade medium containing DAPI stain (ProLong™, Thermo Fisher Scientific). MAP2 and βIII tubulin were used to confirm the isolation of NSCs, and Nrf2 was used to analyze their subcellular localization.

NSC transfection and treatment

NSCs at 1, 2, 5, and 10 μM were treated for 24 h with Aβ1-42 (Sigma-Aldrich, St Louis, MO, United States) dissolved in DMSO; DMSO alone was used as treatment for a control group. Before Aβ1-42 treatment, the NSCs were pretreated with Tan-IIA at doses of 1, 5, 10, 20, and 40 μM for 1 h. The NEAT1 overexpression plasmid (ov-NEAT1), Rab22a small interfering RNAs (siRNAs) (si-Rab22a-1, si-Rab22a-2, and si-Rab22a-3), and miR-291a-3p mimic/inhibitor were purchased from Sangon Biotech Co., Ltd. (Shanghai, China) and transfected into the NSCs (following their Aβ1-42 treatment) using Lipofectamine 3000 Reagent (Invitrogen, Waltham, MA, United States); all the relevant sequences are listed in Table 1.

Hematoxylin and eosin staining

Mouse brains were sectioned into 5 μm thick slices, which were immersed in paraffin and preserved in 4% paraformaldehyde. The sections were deparaffinized, rehydrated, and submitted to hematoxylin and eosin (HE) staining. Histological images were captured at a 400 × magnification using an Olympus light microscope (IX73, Olympus, Shinjuku, Tokyo, Japan).

Enzyme-linked immunosorbent assay

Enzyme-linked immunosorbent assay (ELISA) kits (Solarbio) were used in accordance with the manufacturer's instructions to determine the levels of malondialdehyde (MDA), NO, SOD, GSH, TNF-α, IL-1, and IL-6 in brain tissue homogenates and NSC supernatants. Absorbance was determined at 450 nm using a microplate reader (Thermo Fisher Scientific).

Table 1 Sequences of the three small interfering RNAs targeting *Rab22a* and a microRNA-291a-3p mimic or inhibitor

	Sequences of si-Rab22a 5′-3′
si-Rab22a-1	GGAAATGATCACAAGTAGAGG
si-Rab22a-2	GGAAATGGTAATAAAGACATA
si-Rab22a-3	CGATCTTACTGATGTCAGAGA
si-NC	TTCTCCGAACGTGTCACGTTT
	Sequences of the miR-291a-3p mimic and inhibitor 5′-3′
Mimic NC	ATTGATTTGTTCCGAAGGCCCT
miR-291a-3p mimic	AAAGTGCTTCCACTTTGTGTGC
Inhibitor NC	TCGCTCTATCCTGATCGAATGAA
miR-291a-3p inhibitor	GCACACAAAGTGGAAGCACTTT

Microarray raw dataset analysis

The GSE150696 dataset was analyzed using the DataSet analysis tool (GEO2R, Gene Expression Omnibus 2). The differential expression of lncRNA between the prefrontal cortex of patients with AD and that of elderly individuals without neurological or psychiatric diseases was normalized for log2 |fold change| > 1.5 and $P < 0.05$.

Flow cytometry analysis

Cells were collected, rinsed with phosphate buffered saline, and then resuspended in binding buffer in order to analyze apoptosis. Following the manufacturer's instructions, they were stained with propidium iodide (PI) and Annexin V-fluorescein isothiocyanate (FITC) using an Apoptosis Detection Kit (BD Biosciences, California, United States). Cells were subjected to a 15-min at dark incubation period with Annexin V-FITC and PI at 21 °C, followed by analysis using a BD Biosciences flow cytometry.

ROS measurement

First, 10 M of 2′,7′-dichlorofluorescin (DCF) diacetate (Sigma-Aldrich) was added to the brain tissue homogenates and NSCs lysates, which were then allowed to incubate in the dark for 30 min at 37 °C. The quick oxidation of DCF in the presence of ROS produces extreme fluorescence, of which the intensity was measured with a fluorescence microplate reader (Thermo Fisher Scientific) at excitation and emission wavelengths of 485 and 530 nm, respectively.

Cell viability assay

Following treatment of the NSCs with Aβ1-42 and Tan-IIA, their cell viability was measured using the 3-(4,5-dimethylthiazol-2-yl)-2,5-diphenyltetrazolium bromide (MTT) assay. Briefly, the treated NSCs were seeded into 96-well plates at a density of 3×10^4 cells per well. Each well was supplemented with 20 μL of MTT solution (5 mg/mL), and the plates underwent a 4 h incubation period at 37 °C. After carefully removing the media, DMSO (150 μL) was used to dissolve the formazan crystals that the living cells had generated. Cell viability was then determined (and compared to that of the untreated control group) using a microplate reader to detect absorbance at 570 nm.

Reverse transcription quantitative polymerase chain reaction assay

Total RNA was extracted using TRIzol reagent (Invitrogen). A PrimeScript RT Reagent Kit (Takara Bio, Shiga, Japan) was used to construct complementary DNA from 1 μg of total RNA. Polymerase chain reaction (PCR) was conducted using a QuantStudio 6 Flex Real-Time PCR System (Thermo Fisher Scientific) with SYBR Green PCR Master Mix (Applied Biosystems, CA, United States). Thermal cycling conditions were as follows: 40 cycles of denaturation at 95 °C for 15 s, annealing at 60 °C for 30 s, and extension at 72 °C for 30 s. A preliminary denaturation was then performed at 95 °C for 10 min. The expression levels of NEAT1, Rab22a, and miR-291a-3p were assessed using the $2^{-\Delta\Delta Ct}$ method, with GAPDH or U6 as internal controls for standardization. Primer sequences for all RNAs are shown in Table 2.

Nucleocytoplasmic separation

Nuclear and cytoplasmic fractions were separated according to the manufacturer's instructions using an NE-PER Nuclear and Cytoplasmic Extraction Kit (Thermo Fisher Scientific). The cell pellet was briefly resuspended in CER I buffer obtained from the kit, followed by the addition of CER II buffer. The mixture was vortexed and then rested on ice for an additional 5 min. The cytoplasmic fraction (supernatant) and nuclear pellet were separated from the homogenate *via* centrifugation at 16000 rpm for 5 min at 4° C. The purified nuclear and cytoplasmic fractions were then subjected to reverse transcription quantitative PCR (RT-qPCR).

RNA pull-down assay

Biotin-labeled NEAT1 RNA (bio-NEAT1) and mutant NEAT1 RNA (bio-mut) were synthesized by Sangon Biotech. The NSCs lysates were incubated overnight with bio-NEAT1, bio-mut, or bio-NC at 4 °C. Streptavidin-coated magnetic beads

Table 2 Primer sequences used for reverse transcription quantitative polymerase chain reaction analysis

Primers	Forward primer 5'-3'	Reverse primer 5'-3'
NEAT1	TGGAGATTGAAGGCGCAAGT	AAGCACGGAACCTAGGCAAA
miR-291a-3p	ACACTCCAGCTGGGAAAGTGCTTCCACTTT	CTCAACTGGTGTCGTGGA
U6	CTCGCTTCGGCAGCACA	AACGCTTCACGAATTTGCGT
Rab22a	ATCAATCCAACCATAGGGGCAT	TTGGTGCCAATGCACGAAATC
GAPDH	GTGGCAAAGTGGAGATTGTTGCC	GATGATGACCCGTTTGGCTCC

U6 was used to normalize miR-291a-3p expression, and GAPDH was used to normalize nuclear-enriched abundant transcript 1 mRNA expression. NEAT1: Nuclear-enriched abundant transcript 1.

were added to and incubated with the reaction mixture for 1 h at 4° C to allow the formation of RNA-protein complexes. The beads were then washed, and bound RNA was eluted from them for RT-qPCR analysis to assess enrichment.

Dual-luciferase reporter assay

The miR-291a-3p binding sites from the 3' untranslated regions of NEAT1 and Rab22a were cloned into a psiCHECK-2 dual-luciferase reporter vector (Promega, WI, United States). Using Lipofectamine 3000 reagent (Invitrogen), NSCs were then co-transfected with the reporter plasmids with miR-291a-3p mimic or mimic NC. Luciferase activity was assessed after 48 h using the Dual-Luciferase Reporter Assay System (Promega), in accordance with the manufacturer's instructions. Activity of the *Renilla* luciferase gene was used to normalize firefly luciferase activity.

Western blotting analysis

Total protein was extracted from the mouse brain tissues and NSCs using RIPA lysis buffer (Abcam) along with protease and phosphatase inhibitors (Thermo Fisher Scientific). The protein content was determined using a BCA Protein Assay Kit (Thermo Fisher Scientific). Similar quantities of proteins were separated *via* sodium-dodecyl sulfate gel electrophoresis (Millipore, MA, United States) and then transferred to polyvinylidene fluoride membranes. The membranes were incubated overnight and at 4 °C with primary antibodies (all from Abcam, Cambridge, United Kingdom) against Rab22a (1:1000, ab137093), p65 (1:1000, ab32536), phospho (p)-p65 (1:1000, ab76302), Bax (1:1000, ab32503), Bcl-2 (1:2000, ab182858), and GAPDH (1:2000, ab181602). Next, the membranes were treated with HRP-conjugated secondary antibodies (1:3000, Abcam) for 1 h at 22 °C. Electrochemiluminescence Western Blotting Substrate (NIH, Bethesda, MD, United States) was used to visualize the protein bands, which were quantified using ImageJ software.

Statistical analyses

Data are presented as the mean and standard deviation. GraphPad Prism 8.0 (GraphPad Software, CA, United States) was used for all statistical analyses. One-way analysis of variance was used to evaluate group differences, followed by Tukey's *post-hoc* test. Statistical significance was set at $P < 0.05$.

RESULTS

Tan-IIA ameliorates oxidative stress and inflammatory responses in AD mice

In the healthy control group, neurons were neatly arranged in brain tissues, displaying intact cell structures and clearly visible cell membranes and nuclei. In contrast, the neurons in AD mouse brain tissues showed extreme disarray and irregularities in size and shape, with a drastic reduction in cell number and blurred cell structures. These problems were significantly improved in the treatment group that received 20 mg/kg of Tan-IIA, which proved to be more effective than the 5 mg/kg treatment (Figure 1B). Furthermore, the ELISA showed that Tan-IIA effectively alleviated the elevated oxidative stress (*via* reduced ROS, MDA, and NO and increased SOD and GSH levels) and neuroinflammation (*via* reduced TNF-α, IL-1β, and IL-6 levels) in the AD mouse brain tissue (Figure 1C-J), confirming that 20 mg/kg of Tan-IIA was more effective than 5 mg/kg. A total of 32 associated lncRNAs were identified in the GSE150696 dataset (Table 3), with NEAT1 displaying the highest fold-change to confirm it as a potential therapeutic target (Figure 1K). This lncRNA was both highly expressed in mouse brain tissues and reduced by Tan-IIA treatment (Figure 1L).

Tan-IIA ameliorates Aβ1-42-induced oxidative stress and inflammatory responses in NSCs

To investigate the protective mechanism of Tan-IIA, we isolated mouse NSCs and used Aβ1-42 induction to establish an *in vitro* cellular model of AD. Immunofluorescence results showed substantial positivity for MAP2 and β-III tubulin expression in isolated and cultured NSCs (Figure 2A), indicating successful isolation. Aβ1-42 dose-dependently inhibited NSC viability (Figure 2B), with a subsequent dose of 10 μM Aβ1-42 used for validation. After Tan-IIA pretreatment, doses of 20 and 40 μM reduced NSC viability (Figure 2C); therefore, safe doses of 1, 5, and 10 μM were chosen for subsequent experiments to exclude factors intrinsic to Tan-IIA. The validation results confirmed that Tan-IIA dose-dependently

Table 3 Differentially expressed long non-coding RNAs in the GSE150696 dataset

Gene symbol	Fold change	*P* value
NEAT1	2.19	0.0170
LINC01377	1.98	0.0248
EYA transcriptional coactivator and phosphatase 3- intronic transcript 1	1.95	0.0027
LINC01354	1.68	0.0119
LINC00537	1.64	0.0498
LINC01441	1.63	0.0082
LINC01094	1.63	0.0328
Cancer susceptibility 16	1.6	0.0376
LINC01101	1.55	0.0342
LINC00327	1.54	0.0028
LINC00323	1.54	0.0459
LINC00644	1.53	0.0119
LINC00358	1.53	0.0411
LINC00347	1.51	0.0409
LINC00641	-1.53	0.0332
LINC00294	-1.55	0.0471
Maternally expressed 8	-1.56	0.0073
Prader-Willi region non-protein coding RNA 1	-1.59	0.0005
LINC00672	-1.66	0.0010
LINC00969	-1.72	0.0302
Prostate androgen-regulated transcript 1	-1.8	0.0049
LINC00622	-1.8	0.0175
LINC00507	-1.81	0.0000625
LINC00403	-1.84	0.0043
LINC01128	-1.87	0.0179
LINC00889	-1.92	0.0113
LINC00473	-2.43	0.0323
LINC00622	-2.5	0.0037

LINC: Long intergenic long non-coding RNA; NEAT1: Nuclear-enriched abundant transcript 1.

ameliorated Aβ1-42-induced reductions in cell viability (Figure 2D), apoptosis (Figure 2E), oxidative stress (increased ROS, MDA, and NO; decreased SOD and GSH) and increases in neuroinflammatory markers (TNF-α, IL-1β, and IL-6) (Figure 2F-N). In the process, the Aβ1-42-induced expression of NEAT1 lncRNA was suppressed (Figure 2O). For subsequent mechanistic studies, a safe dose of 10 μM Tan-IIA was selected, as it ameliorated Aβ1-42-induced effects most efficiently.

LncRNA NEAT1 reverses the improvements of Tan-IIA treated Aβ1-42-induced NSCs via miR-291a-3p

Nucleocytoplasmic separation experiments revealed that the lncRNA NEAT1 was abundantly expressed in the cytoplasm, a result similar to that observed in the positive control GAPDH and opposite to that of U6 (Figure 3A). In verifying the efficacy of the constructed ov-NEAT1 (Figure 3B), it was observed that it partially counteracted the protective effect of Tan-IIA preconditioning on NSCs, partially reversing the Tan-IIA improvement of Aβ1-42-inhibited cell viability (Figure 3C), promoted apoptosis (Figure 3D), oxidative stress (increased ROS, MDA, and NO levels; decreased SOD and GSH levels) and neuroinflammation (increased TNF-α, IL-1β, and IL-6) (Figure 3E-L). A joint analysis using Starbase and Lncbase identified miR-291a-3p as a potential target of NEAT1 (Figure 3M), which was confirmed to be one of the key miRNAs in ameliorating AD[28]. Indeed, miR-291a-3p was downregulated in both the *in vivo* and *in vitro* models of AD and upregulated upon Tan-IIA treatment (Figure 3N and O), further supporting this hypothesis. After

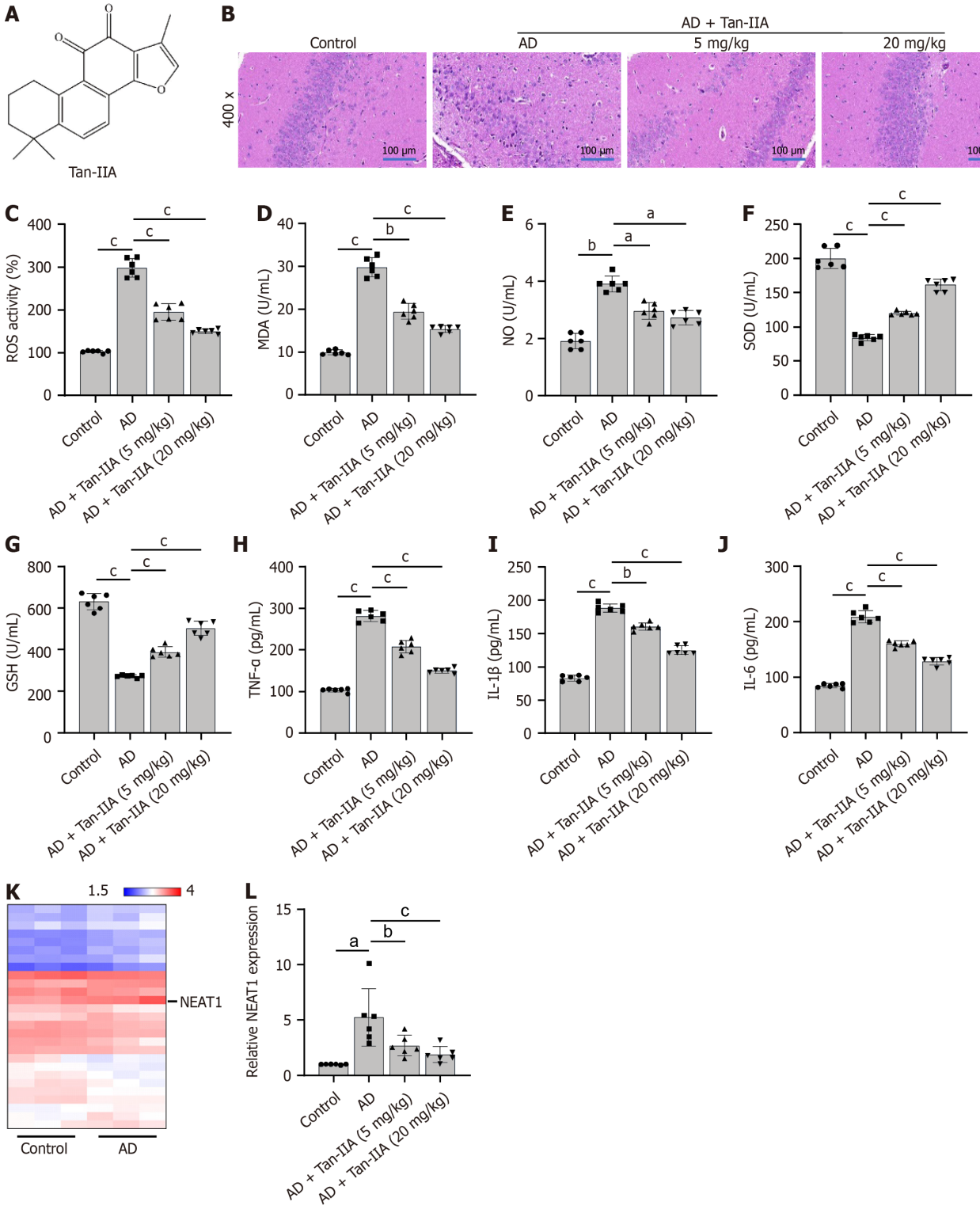

Figure 1 The impact of tanshinone IIA in a murine model of Alzheimer's disease, with the long non-coding RNA nuclear-enriched abundant transcript 1 as a potential target. A: Chemical structure of tanshinone IIA (Tan-IIA); B: Hematoxylin and eosin staining of brain tissues from control, Alzheimer's disease, and Tan-IIA-treated mice (400 × magnification); C: Results of the 2',7'-dichlorofluorescin diacetate analysis of the reactive oxygen species ratio in mouse brain tissues, either with or without prior Tan-IIA treatment; D-J: Enzyme-linked immunosorbent assay analysis of oxidative stress factors (malondialdehyde; nitric oxide; superoxide dismutase; glutathione) and neuroinflammation markers (tumor necrosis factor-alpha; interleukin 1β; interleukin 6) in mouse brain tissues; K: GEO2R web tool analysis of the GSE150696 data set for long non-coding RNA screening; L: Analysis the expression of nuclear-enriched abundant transcript 1 in Tan-IIA-treated mouse brain tissues. $^{a}P < 0.05$, $^{b}P < 0.01$, $^{c}P < 0.001$. AD: Alzheimer's disease; Tan-IIA: Tanshinone IIA; ROS: Reactive oxygen species; MDA: Malondialdehyde; NO: Nitric oxide; SOD: Superoxide dismutase; GSH: Glutathione; TNF-α: Tumor necrosis factor-alpha; IL-1β: Interleukin 1β; IL-6: Interleukin 6.

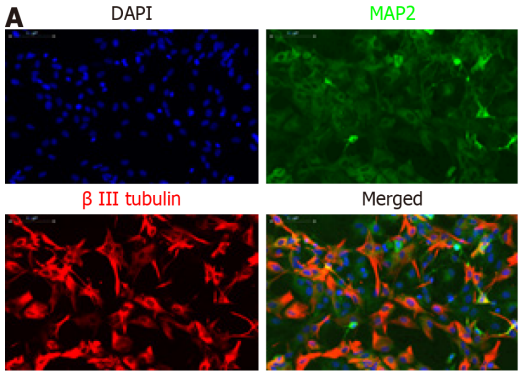
A
DAPI
MAP2
β III tubulin
Merged

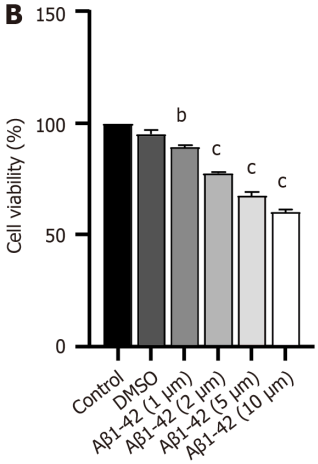
B
Cell viability (%)
150
100
50
0
b
c
c
c
Control
DMSO
Aβ1-42 (1 μm)
Aβ1-42 (2 μm)
Aβ1-42 (5 μm)
Aβ1-42 (10 μm)

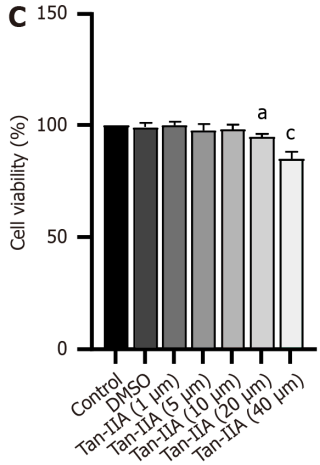
C
Cell viability (%)
150
100
50
0
a
c
Control
DMSO
Tan-IIA (1 μm)
Tan-IIA (5 μm)
Tan-IIA (10 μm)
Tan-IIA (20 μm)
Tan-IIA (40 μm)

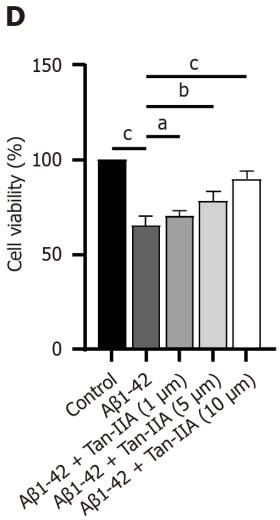
D
Cell viability (%)
150
100
50
0
c
b
a
c
Control
Aβ1-42
Aβ1-42 + Tan-IIA (1 μm)
Aβ1-42 + Tan-IIA (5 μm)
Aβ1-42 + Tan-IIA (10 μm)

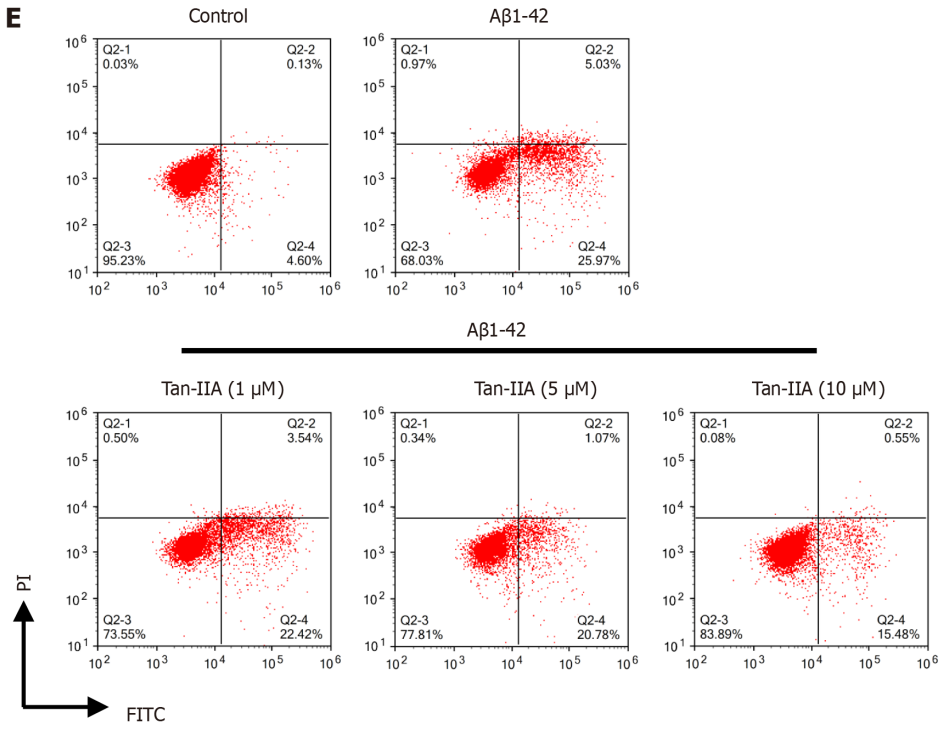
E
Control
Aβ1-42
Q2-1 0.03%
Q2-2 0.13%
Q2-3 95.23%
Q2-4 4.60%
Q2-1 0.97%
Q2-2 5.03%
Q2-3 68.03%
Q2-4 25.97%
Aβ1-42
Tan-IIA (1 μM)
Tan-IIA (5 μM)
Tan-IIA (10 μM)
Q2-1 0.50%
Q2-2 3.54%
Q2-3 73.55%
Q2-4 22.42%
Q2-1 0.34%
Q2-2 1.07%
Q2-3 77.81%
Q2-4 20.78%
Q2-1 0.08%
Q2-2 0.55%
Q2-3 83.89%
Q2-4 15.48%
PI
FITC

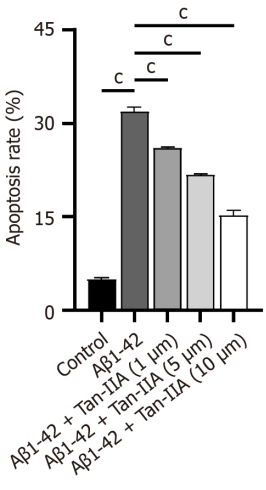
Apoptosis rate (%)
45
30
15
0
c
c
c
c
Control
Aβ1-42
Aβ1-42 + Tan-IIA (1 μm)
Aβ1-42 + Tan-IIA (5 μm)
Aβ1-42 + Tan-IIA (10 μm)

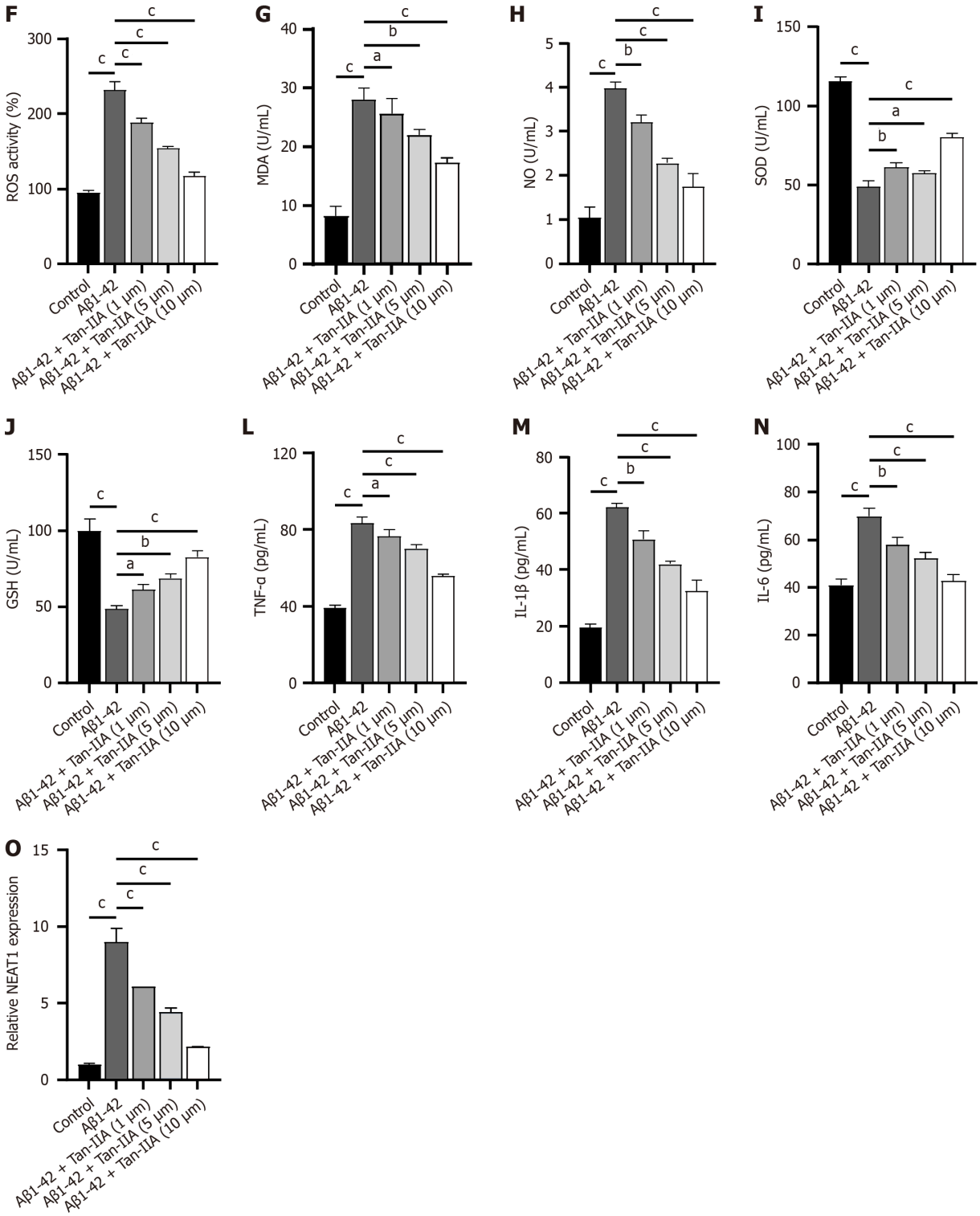

Figure 2 Protective effects of tanshinone IIA in murine neural stem cells induced with amyloid-beta 1-42 peptides. A: Immunofluorescent identification of neural stem cells (NSCs) for isolation, using DAPI stain (blue), microtubule-associated protein 2 (green), and β III tubulin (red); B-D: 3-(4,5-dimethylthiazol-2-yl)-2,5-diphenyltetrazolium bromide assay of the effect of different amyloid-beta 1-42 (Aβ1-42) and tanshinone IIA (Tan-IIA) doses on NSC viability; E: Flow cytometry results indicating that different Tan-IIA doses improve the effect of Aβ1-42 on the apoptosis of NSCs; F: 2',7'-dichlorofluorescin diacetate analysis of the reactive oxygen species ratio in NSCs, either with or without prior Tan-IIA treatment; G-N: Enzyme-linked immunosorbent assay results of different Tan-IIA doses in enhancing the effect of Aβ1-42 in improving levels of oxidative stress factors (malondialdehyde; nitric oxide; superoxide dismutase; glutathione) and neuroinflammation markers (tumor necrosis factor-alpha; interleukin 1β; interleukin 6) in NSCs; O: Reverse transcription quantitative polymerase chain reaction analysis of different Tan-IIA doses used to improve the effect of Aβ1-42 on nuclear-enriched abundant transcript 1 expression in NSCs. $^{a}P < 0.05$, $^{b}P < 0.01$, $^{c}P < 0.001$. MAP2: Microtubule-associated protein 2; DMSO: Dimethyl sulfoxide; PI: Propidium iodide; FITC: Fluorescein isothiocyanate; Aβ1-42: Amyloid-beta 1-42; Tan-IIA: Tanshinone IIA; ROS: Reactive oxygen species; MDA: Malondialdehyde; NO: Nitric oxide; SOD: Superoxide dismutase; GSH: Glutathione; TNF-α: Tumor necrosis factor-alpha; IL-1β: Interleukin 1β; IL-6: Interleukin 6; NEAT1: Nuclear-enriched abundant transcript 1.

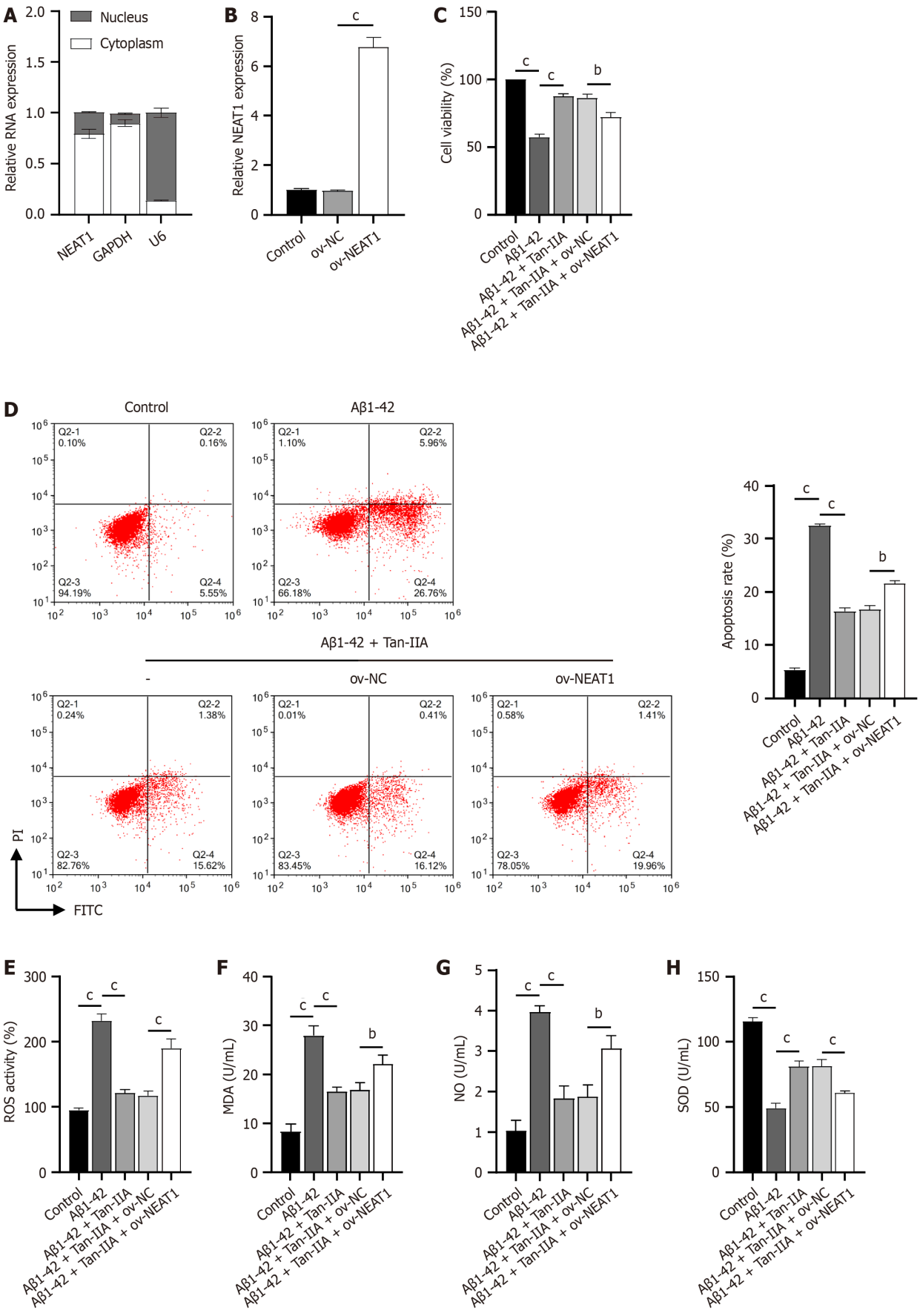
A
Nucleus
Cytoplasm
Relative RNA expression
NEAT1
GAPDH
U6
B
Relative NEAT1 expression
Control
ov-NC
ov-NEAT1
C
Cell viability (%)
Control
Aβ1-42
Aβ1-42 + Tan-IIA
Aβ1-42 + Tan-IIA + ov-NC
Aβ1-42 + Tan-IIA + ov-NEAT1
D
Control
Aβ1-42
Aβ1-42 + Tan-IIA
-
ov-NC
ov-NEAT1
Q2-1 0.10%
Q2-2 0.16%
Q2-3 94.19%
Q2-4 5.55%
Q2-1 1.10%
Q2-2 5.96%
Q2-3 66.18%
Q2-4 26.76%
Q2-1 0.24%
Q2-2 1.38%
Q2-3 82.76%
Q2-4 15.62%
Q2-1 0.01%
Q2-2 0.41%
Q2-3 83.45%
Q2-4 16.12%
Q2-1 0.58%
Q2-2 1.41%
Q2-3 78.05%
Q2-4 19.96%
PI
FITC
Apoptosis rate (%)
E
ROS activity (%)
F
MDA (U/mL)
G
NO (U/mL)
H
SOD (U/mL)

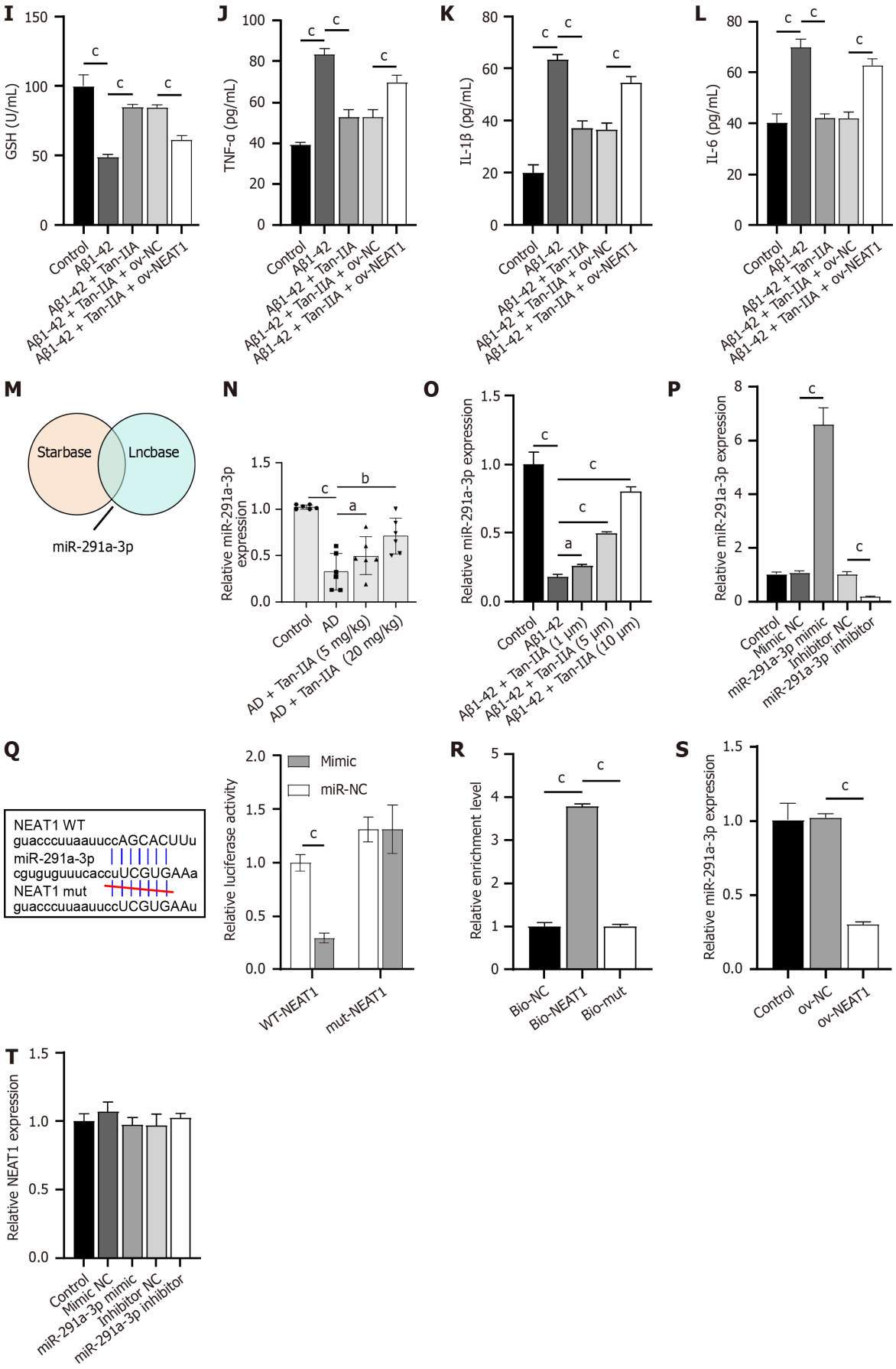

Figure 3 Localization of the long non-coding RNA nuclear-enriched abundant transcript 1 in the cytoplasm, and its interaction with the microRNA miR-291a-3p. A: Nucleocytoplasmic separation was performed to detect the localization of the long non-coding RNA nuclear-enriched abundant

transcript 1 (NEAT1) in neural stem cells (NSCs); B: Reverse transcription quantitative polymerase chain reaction validation of the NEAT1 overexpression vector; C: 3-(4,5-dimethylthiazol-2-yl)-2,5-diphenyltetrazolium bromide results of the effect of NEAT1 overexpression on the cell viability of amyloid-beta 1-42 (Aβ1-42)-induced NSCs that received tanshinone IIA (Tan-IIA) pretreatment; D: Flow cytometry results of the effect of NEAT1 overexpression on the apoptosis of Aβ1-42-induced NSCs that received Tan-IIA pretreatment; E: 2',7'-dichlorofluorescin diacetate analysis of the effect of NEAT1 overexpression on the reactive oxygen species ratio of Aβ1-42-induced NSCs that received Tan-IIA pretreatment; F–L: Enzyme-linked immunosorbent assay results for the effect of NEAT1 overexpression on oxidative stress factors (malondialdehyde; nitric oxide; superoxide dismutase; glutathione) and neuroinflammation markers (tumor necrosis factor-alpha; interleukin 1β; interleukin 6) in Aβ1-42-induced NSCs that received Tan-IIA pretreatment; M: Starbase and Lncbase analysis, confirming miR-291a-3p as a potential target of NEAT1; N and O: Reverse transcription quantitative polymerase chain reaction (RT-qPCR) analysis of miR-291a-3p expression in the Alzheimer's disease mouse model and Aβ1-42-induced NSCs; P: RT-qPCR analysis of the expression of synthesized miR-291a-3p mimic/inhibitor; Q: Dual-luciferase assay confirming binding between NEAT1 and miR-291a-3p; R: RNA pull-down assay showing miR-291a-3p enrichment in bio-NEAT1; S and T: RT-qPCR analysis of the expression levels of miR-291a-3p (S) and NEAT1 (T) in NSCs. $^{a}P < 0.05$, $^{b}P < 0.01$, $^{c}P < 0.001$. PI: Propidium iodide; FITC: Fluorescein isothiocyanate; Aβ1-42: Amyloid-beta 1-42; Tan-IIA: Tanshinone IIA; ROS: Reactive oxygen species; MDA: Malondialdehyde; NO: Nitric oxide; SOD: Superoxide dismutase; GSH: Glutathione; TNF-α: Tumor necrosis factor-alpha; IL-1β: Interleukin 1β; IL-6: Interleukin 6; NEAT1: Nuclear-enriched abundant transcript 1.

confirming the efficacy of the synthesized miR-291a-3p mimic and inhibitor (Figure 3P), a dual-luciferase assay was performed. The fluorescence activity in the WT-NEAT1 and miR-291a-3p mimic co-transfected group was significantly lower than that in the WT-NEAT1 and mimic NC co-transfected group, whereas there was no significant difference in fluorescence activity between the mut-NEAT1 and miR-291a-3p mimic or mimic NC co-transfected groups (Figure 3Q). RNA pull-down results showed significant enrichment of miR-291a-3p in bio-NEAT1, with no discernible differences in its expression between the bio-mut and bio-NC groups (Figure 3R). Overexpression of NEAT1 significantly suppressed miR-291a-3p expression (Figure 3S). However, changes in miR-291a-3p expression had no apparent effect on NEAT1 expression (Figure 3T). These results confirm that NEAT1 directly targets and binds to miR-291a-3p.

Rab22a is a direct target of miR-291a-3p

Joint analysis using miRDB and TargetScan databases identified Rab22a, an inhibitor of the AKT pathway, as a potential target of miR-291a-3p (Figure 4A). Rab22a expression increased in both the *in vivo* and *in vitro* models and decreased upon Tan-IIA treatment (Figure 4B-D). Dual-luciferase assay results showed that luminescence activity was significantly lower in the WT-NEAT1 and miR-291a-3p mimic co-transfection group than in the WT-Rab22a and NC mimic co-transfection groups, and no significant effects on luminescence activity were found between the mut-Rab22a and miR-291a-3p mimic or NC mimic co-transfection groups (Figure 4E). In addition, Rab22a expression was negatively regulated by miR-291a-3p (Figure 4F) and increased upon NEAT1 overexpression (Figure 4G). Therefore, Rab22a may be a potential target of miR-291a-3p. Among the constructed siRNAs, si-Rab22a-1 was selected for further study because of its high Rab22a silencing efficiency in NSCs (Figure 4H) and because the expression of si-Rab22a did not significantly affect miR-291a-3p (Figure 4I).

Tan-IIA inhibits oxidative stress and neuroinflammation by activating AKT/Nrf2 signaling through the NEAT1/miR-291a-3p/Rab22a axis

To investigate the protective mechanism of Tan-IIA against Aβ1-42-induced damage, the miR-291a-3p mimic, ov-NEAT1, and si-Rab22a were co-transfected into NSCs. As expected, Tan-IIA ameliorated the Aβ1-42-induced reduction in cell viability, promoted apoptosis, oxidative stress (increased ROS, MDA, and NO levels; decreased SOD and GSH levels), and neuroinflammation (increased TNF-α, IL-1β, and IL-6) (Figure 5A-J). The miR-291a-3p mimic enhanced the effects of Tan-IIA, whereas ov-NEAT1 counteracted or partially counteracted the effects of the miR-291a-3p mimic. However, these effects were reversed by si-Rab22a treatment (Figure 5A-J). Notably, the total p65 protein level was unchanged, and p65 phosphorylation and Bax protein levels were opposite to those of RAB22A and Bcl-2. Tan-IIA reduced Aβ1-42-induced p65 phosphorylation and Bax activation, and the miR-291a-3p mimic further enhanced these effects. In addition, the counteracting effects of ov-NEAT1 on that of miR-291a-3p were inhibited by si-RAB22A (Figure 5K), and the Bcl-2/Bax ratio was consistent with that of Bcl-2. Similar to the *in vitro* results, Tan-IIA reduced p65 phosphorylation and Bax activation and increased Bcl-2 levels in AD mice *in vivo*. The enhancing effects of the miR-291a-3p mimic on Tan-IIA were counteracted by NEAT1, but inhibited by si-RAB22A (Figure 5L), and the ratio of Bcl-2/Bax was consistent with that of Bcl-2.

DISCUSSION

Studies have shown that the dysregulation of lncRNAs - such as lung adenocarcinoma transcripts 1 and NEAT1, which are associated with metastasis - can be critical in the pathogenesis of many degenerative diseases[29-31], including AD. In this study, we investigated the neuroprotective effects of Tan-IIA using both *in vivo* and *in vitro* (Aβ1-42-induced NSCs) models of AD to elucidate the underlying mechanisms involving the lncRNA NEAT1/miR-291a-3p/Rab22a signaling axis.

Consistent with previous reports, our results showed that Tan-IIA treatment significantly ameliorated AD-induced histopathological changes, reduced oxidative stress, and attenuated neuroinflammation in the brain tissue of AD mice[26, 32]. In particular, the dose-dependent improvements observed in Aβ1-42-induced NSCs *in vitro* supported the potential of Tan-IIA as a promising AD therapeutic agent. During this process, the expression of NEAT1 - a promising key

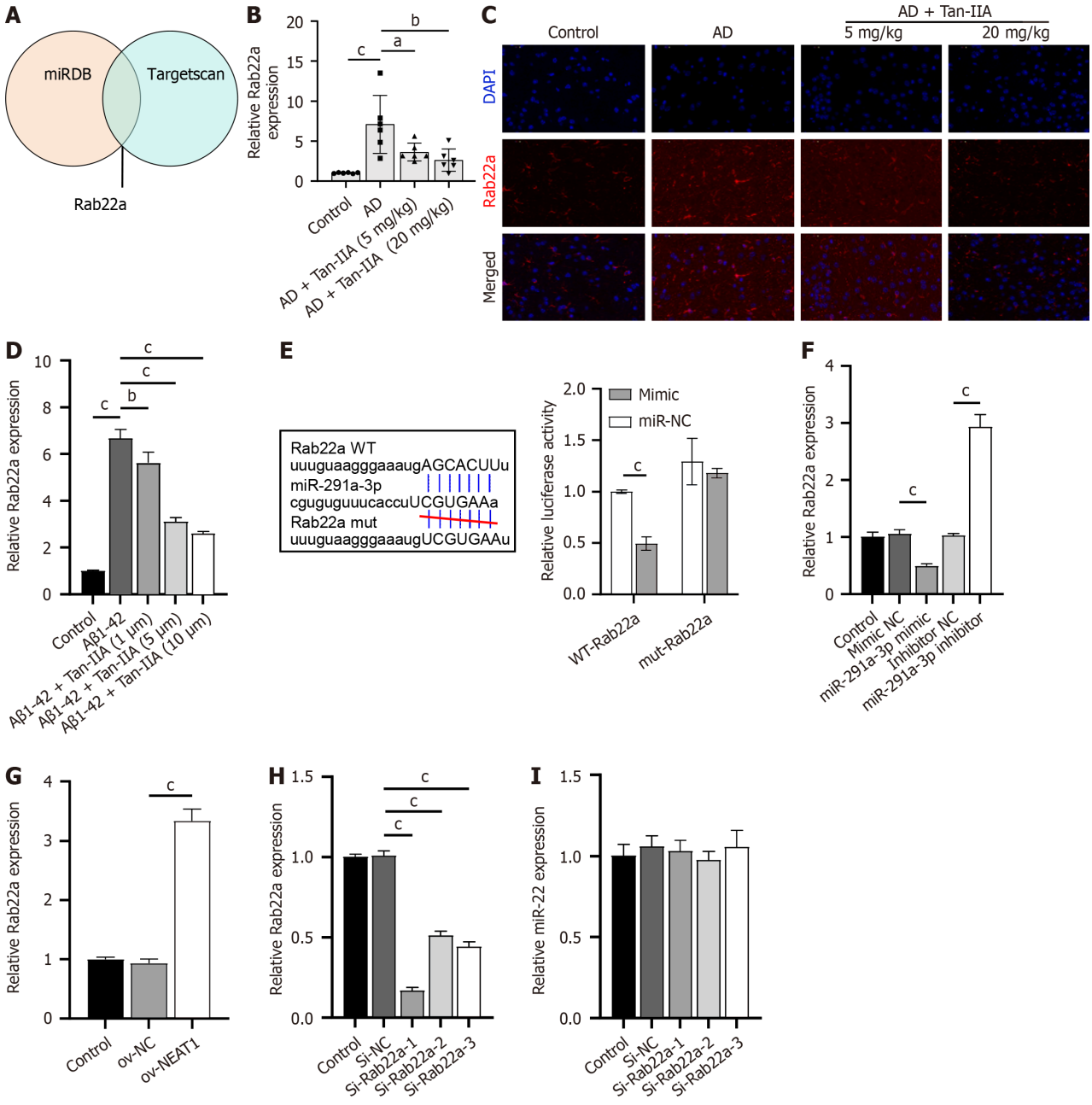

Figure 4 Rab22a as a target of miR-291a-3p, and its role in the nuclear-enriched abundant transcript 1/miR-291a-3p axis. A: MiRDB and Targetscan database joint analysis identified Rab22a as a potential target of miR-291a-3p; B: Reverse transcription quantitative polymerase chain reaction (RT-qPCR) analysis of Rab22a expression in the Alzheimer's disease (AD) mouse model; C: Immunofluorescence analysis of Rab22a expression in the AD mouse model; D: RT-qPCR analysis of Rab22a expression in amyloid-beta 1-42 (Aβ1-42)-induced neural stem cells (NSCs); E: Dual-luciferase assay confirming binding between Rab22a and miR-291a-3p; F and G: RT-qPCR analysis of the effect of miR-291a-3p (F) and nuclear-enriched abundant transcript 1 (G) overexpression on Rab22a expression; H: RT-qPCR validation of the inhibitory efficiency of 3 si-Rab22a on Rab22a expression in NSCs; I: RT-qPCR analysis of the effect of 3 si-Rab22a on miR-291a-3p expression. $^{a}P < 0.05$, $^{b}P < 0.01$, $^{c}P < 0.001$. AD: Alzheimer's disease; Aβ1-42: Amyloid-beta 1-42; Tan-IIA: Tanshinone IIA.

therapeutic target lncRNA obtained from the GSE150696 dataset analysis - was suppressed in a Tan-IIA dose-dependent manner, suggesting its possible involvement in the protective mechanism of Tan-IIA. Indeed, NEAT1 has been shown to be one of the major lncRNAs that exacerbate AD[33]. This hypothesis was confirmed in our observation that an overexpression of NEAT1 counteracted the ameliorative effect of Tan-IIA on Aβ1-42 induction. This is the first time that the ameliorative effect of Tan-IIA in alleviating AD symptoms has been linked to NEAT1, suggesting the possibility of a new regulatory axis for subsequent lncRNAs, which is important for the development of new therapeutic strategies against AD.

We further revealed a direct interaction between NEAT1 and miR-291a-3p, an important player in nerve injury[34]. Our results show that NEAT1 acts as a sponge for miR-291a-3p, thereby regulating miR-291a-3p availability and function, which is the first confirmation that miR-291a-3p contributes to the regulation of AD mitigation. We also confirmed that Rab22a, a regulator of activated NF-κB signaling, is a direct target of miR-291a-3p. This finding is notable because it is the first time that Tan-IIA regulation of Rab22a *via* the NEAT1/miR-291a-3p axis has been shown to reduce the activation of

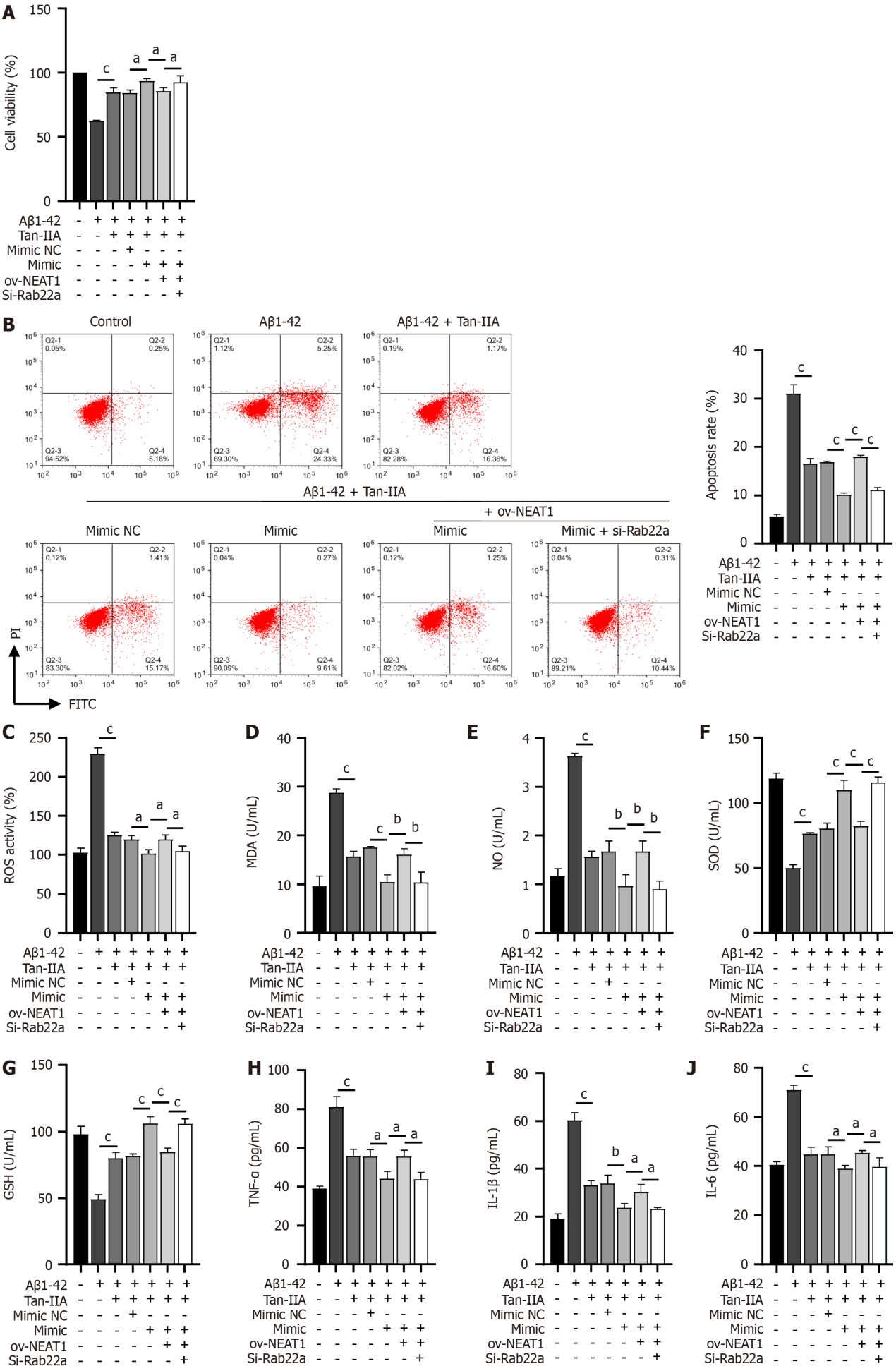
A
Cell viability (%)
Aβ1-42
Tan-IIA
Mimic NC
Mimic
ov-NEAT1
Si-Rab22a
B
Control
Aβ1-42
Aβ1-42 + Tan-IIA
Mimic NC
Mimic
+ ov-NEAT1
Mimic + si-Rab22a
PI
FITC
Apoptosis rate (%)
C
ROS activity (%)
D
MDA (U/mL)
E
NO (U/mL)
F
SOD (U/mL)
G
GSH (U/mL)
H
TNF-α (pg/mL)
I
IL-1β (pg/mL)
J
IL-6 (pg/mL)

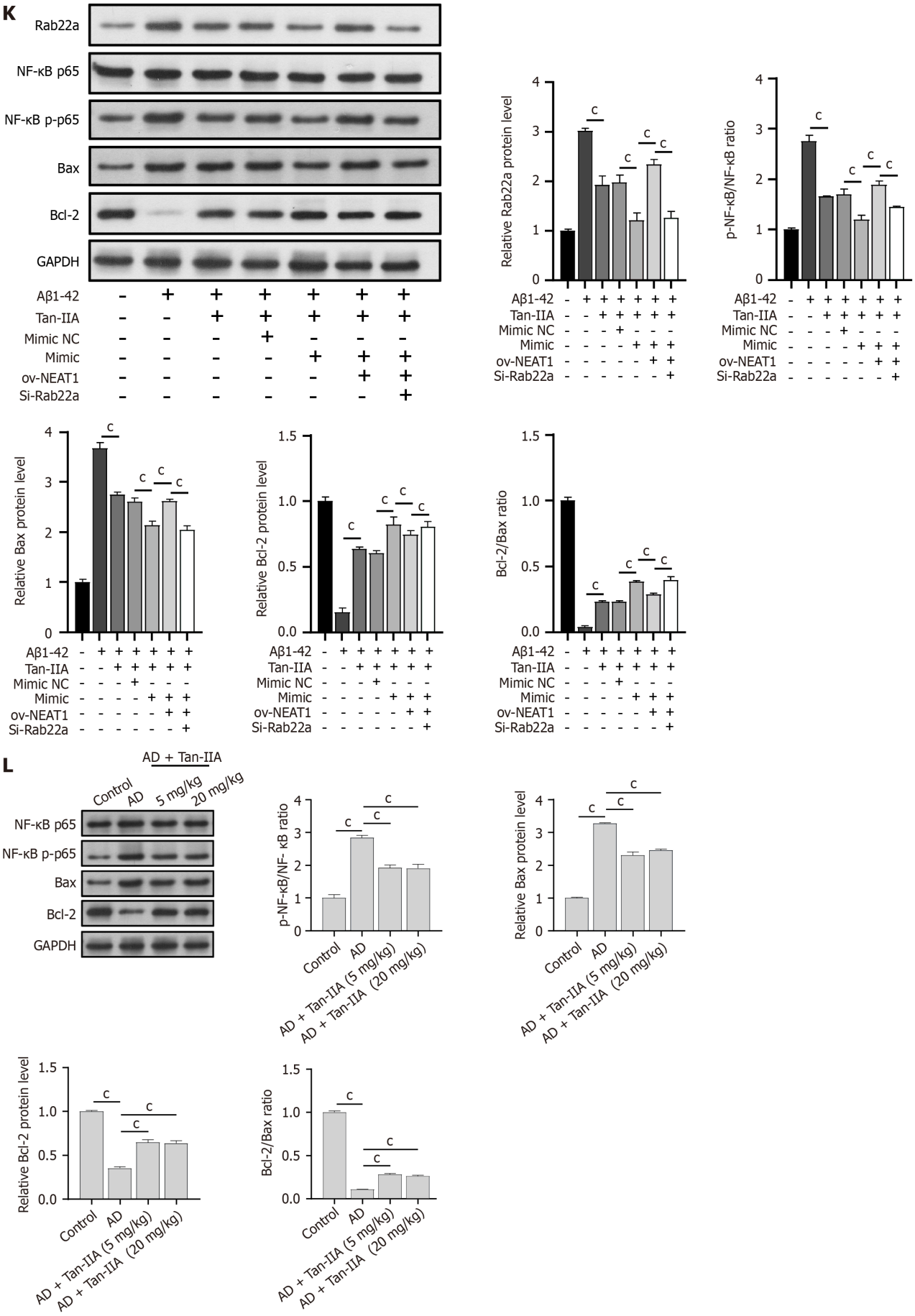

Figure 5 Neuroprotective effects of tanshinone IIA as mediated through the nuclear-enriched abundant transcript 1/miR-291a-3p/Rab22a

axis. A: 3-(4,5-dimethylthiazol-2-yl)-2,5-diphenyltetrazolium bromide analysis of the role of nuclear-enriched abundant transcript 1 (NEAT1)/miR-291a-3p/Rab22a axis in the improvement of cell viability in amyloid-beta 1-42 (Aβ1-42)-induced neural stem cells (NSCs) following tanshinone IIA (Tan-IIA) treatment; B: Flow cytometry analysis of the role of the NEAT1/miR-291a-3p/Rab22a axis in Tan-IIA ameliorating Aβ1-42-induced apoptosis in NSCs; C: 2',7'-dichlorofluorescin diacetate analysis of the role of the NEAT1/miR-291a-3p/Rab22a axis in Tan-IIA ameliorating Aβ1-42-induced reactive oxygen species levels in NSCs; D-J: Enzyme-linked immunosorbent assay analysis of the role of NEAT1/miR-291a-3p/Rab22a axis in Tan-IIA to ameliorate oxidative stress factors (malondialdehyde; nitric oxide; superoxide dismutase; and glutathione) and neuroinflammation (tumor necrosis factor-alpha; interleukin 1β; and interleukin 6) in Aβ1-42-induced NSCs; K: Western blots indicating the role of the NEAT1/miR-291a-3p/Rab22a axis in the mechanism of Tan-IIA improving the role of Rab22a, p65, p-p65, Bax, and Bcl-2 protein levels in NSCs induced by Aβ1-42; L: Western blots showing the effect of Tan-IIA treatment on the protein levels of p65, p-p65, B-cell lymphoma 2-associated X protein, and B-cell lymphoma 2 in AD mice. $^{a}P < 0.05$, $^{b}P < 0.01$, $^{c}P < 0.001$. PI: Propidium iodide; FITC: Fluorescein isothiocyanate; Aβ1-42: Amyloid-beta 1-42; Tan-IIA: Tanshinone IIA; ROS: Reactive oxygen species; MDA: Malondialdehyde; NO: Nitric oxide; SOD: Superoxide dismutase; GSH: Glutathione; TNF-α: Tumor necrosis factor-alpha; IL-1β: Interleukin 1β; IL-6: Interleukin 6; NEAT1: Nuclear-enriched abundant transcript 1; NF-κB: Nuclear factor kappa-B; Bcl-2: B-cell lymphoma 2; Bax: B-cell lymphoma 2-associated X protein; AD: Alzheimer's disease.

NF-κB signaling, a key pathway involved in oxidative stress, neuroinflammation and cell survival in AD. This was confirmed by changes in the levels of factors related to oxidative stress and neuroinflammation. Therefore, we identified the NEAT1/miR-291a-3p/Rab22a axis as an important signaling axis for the Tan-IIA-mediated amelioration of oxidative stress and neuroinflammation levels in both *in vivo* and *in vitro* models of AD.

The activation of NF-κB signaling is known to lead to altered activation of the downstream pro- and anti-apoptotic proteins, Bax and Bcl-2[35,36]. In the present study, we observed that Tan-IIA inhibited NF-κB signaling, leading to reduced levels of the pro-apoptotic Bax and activation of the anti-apoptotic Bcl-2 proteins in both our *in vivo* and *in vitro* models of AD. The ratio of Bcl-2/Bax was consistent with that of Bcl-2, and these results corresponded to its amelioration of Aβ1-42- induced apoptosis in NSCs, which increases our understanding of the role of Tan-IIA in the mechanism of AD. This study has several limitations. First, it presents no clinical data to confirm the roles of Tan-IIA and NEAT1 in patients with AD. Second, many lncRNAs have not yet been analyzed and verified through GEO data mining. Third, this study was the first to propose miR-291a-3p and Rab22a as novel therapeutic targets for AD, which requires further validation. Finally, our focusing on the NEAT1/miR-291a-3p/Rab22a axis may have overlooked alternative molecular pathways that contribute to the neuroprotective effects of Tan-IIA. The directions and goals of future research should aim to bridge these research gaps.

CONCLUSION

This study revealed the potential therapeutic role of Tan-IIA in AD by demonstrating its ability to attenuate oxidative stress and neuroinflammation in a mouse model and in Aβ1-42-induced murine NSCs. By elucidating the involvement of the NEAT1/miR-291a-3p/Rab22a signaling axis in the neuroprotective effects of Tan-IIA, this research not only deepens our understanding of the molecular mechanisms underlying AD but also highlights a promising target for the development of new therapeutic strategies.

ARTICLE HIGHLIGHTS

Research background

Alzheimer's disease (AD) is a prevalent neurodegenerative disorder characterized by cognitive decline and neuronal loss. Oxidative stress and neuroinflammation play pivotal roles in the pathogenesis of this disease. Tanshinone IIA (Tan-IIA), which is derived from *Salvia miltiorrhiza*, shows potential neuroprotective effects. Understanding the molecular mechanisms underlying these effects is crucial for the development of novel therapeutic strategies.

Research motivation

The motivation for this study was to elucidate the mechanisms by which Tan-IIA exerts neuroprotective effects in AD, focusing on the potential modulation of the long non-coding RNA (lncRNA) nuclear enriched abundant transcript 1 (NEAT1), microRNA (miR)-291a-3p, and RAB22A, member of the RAS oncogene family (Rab22a) signaling pathways. This has important implications for the development of new AD therapies.

Research objectives

The objective of this study was to investigate the neuroprotective effects of Tan-IIA in AD models and elucidate the underlying molecular mechanisms. Specifically, we aimed to determine how Tan-IIA affects oxidative stress, neuroinflammation, and neuronal viability through the NEAT1/miR-291a-3p/Rab22a signaling axis.

Research methods

The study employed both *in vivo* and *in vitro* models of AD using mice and neural stem cells, respectively. Methods included histopathological examinations, enzyme-linked immunosorbent assays, western blotting, 3-(4,5-dimethylthiazol-

2-yl)-2,5-diphenyltetrazolium bromide assays, reverse transcription quantitative polymerase chain reaction assays, and various molecular biology techniques to elucidate the role of the NEAT1/miR-291 a-3p/Rab22a pathway in mediating the effects of Tan-IIA.

Research results

Tan-IIA ameliorated AD-related pathological changes, reduced oxidative stress, and attenuated neuroinflammation in the mouse models. It modulated the expression of NEAT1, miR-291a-3p, and Rab22a, indicating the involvement of this signaling axis in its neuroprotective effects. This is the first study to link the amelioration of AD symptoms by Tan-IIA with the downregulation of NEAT1.

Research conclusions

Tan-IIA has potential therapeutic roles in AD by attenuating oxidative stress and neuroinflammation, primarily through the NEAT1/miR-291a-3p/Rab22a signaling axis. This highlights the intricate molecular interplay involved in AD and identifies lncRNAs and miRNAs as potential therapeutic targets.

Research perspectives

Future research should focus on validating the identified therapeutic targets, namely miR-291a-3p and Rab22a, in clinical AD models. It is also crucial to explore other potential molecular pathways affected by Tan-IIA to fully understand its neuroprotective mechanisms. Clinical trials are essential to determine the efficacy and safety of Tan-IIA-based therapies in patients with AD. Expanding our understanding of the role of NEAT1 in AD could open new avenues for RNA-based therapeutic strategies.

FOOTNOTES

Author contributions: Yang LX, Luo M, and Li SY contributed to the study design, experiments, data collection, and manuscript writing; Luo M and Li SY contributed to the visualization; Li SY contributed to the resources; and all authors have read and approved the final manuscript.

Supported by 2020 Guangxi Zhuang Autonomous Region Health Care Commission Self-Financing Research Projects, No. Z20200096; 2023 Guangxi University Young and Middle-Aged Teachers' Basic Research Ability Improvement Project, No. 2023KY0091; National Natural Science Foundation of China, No. 82260241; and the Natural Science Foundation of Guangxi Province, No. 2015GXNSFAA139171 and No. 2020GXNSFAA259053.

Institutional animal care and use committee statement: All procedures involving animals were approved by the Animal Care and Use Committee of the First Affiliated Hospital of Guangxi Medical University, No. 2021(KY-E-292), and performed in accordance with the Guide for the Care and Use of Laboratory Animals. All surgery and euthanasia were performed under sodium pentobarbital anesthesia (200 mg/kg) by intraperitoneal injection, and all efforts were made to minimize suffering.

Conflict-of-interest statement: All the authors report no relevant conflicts of interest for this article.

Data sharing statement: The datasets used and/or analyzed in the current study are available from the corresponding author upon reasonable request.

ARRIVE guidelines statement: The authors have read the ARRIVE guidelines, and the manuscript was prepared and revised according to the ARRIVE guidelines.

Country/Territory of origin: China

ORCID number: Sheng-Yu Li 0009-0005-7369-7528.

S-Editor: Wang JJ
L-Editor: A
P-Editor: Zhao S

REFERENCES

1 **Gibbs DM**. Alzheimer's dementia or Alzheimer's disease - What's the difference and why should we care? *Ageing Res Rev* 2022; **82**: 101779 [PMID: 36332757 DOI: 10.1016/j.arr.2022.101779]

2 **Graff-Radford J**, Yong KXX, Apostolova LG, Bouwman FH, Carrillo M, Dickerson BC, Rabinovici GD, Schott JM, Jones DT, Murray ME. New insights into atypical Alzheimer's disease in the era of biomarkers. *Lancet Neurol* 2021; **20**: 222-234 [PMID: 33609479 DOI: 10.1016/S1474-4422(20)30440-3]

3 **Xiao L**, Yang X, Sharma VK, Abebe D, Loh YP. Hippocampal delivery of neurotrophic factor-α1/carboxypeptidase E gene prevents neurodegeneration, amyloidosis, memory loss in Alzheimer's Disease male mice. *Mol Psychiatry* 2023; **28**: 3332-3342 [PMID: 37369719 DOI: 10.1038/s41380-023-02135-7]

4 **Tiwari S**, Atluri V, Kaushik A, Yndart A, Nair M. Alzheimer's disease: pathogenesis, diagnostics, and therapeutics. *Int J Nanomedicine* 2019; **14**: 5541-5554 [PMID: 31410002 DOI: 10.2147/IJN.S200490]

5 **DeTure MA**, Dickson DW. The neuropathological diagnosis of Alzheimer's disease. *Mol Neurodegener* 2019; **14**: 32 [PMID: 31375134 DOI: 10.1186/s13024-019-0333-5]

6 **Rajendran L**, Paolicelli RC. Microglia-Mediated Synapse Loss in Alzheimer's Disease. *J Neurosci* 2018; **38**: 2911-2919 [PMID: 29563239 DOI: 10.1523/JNEUROSCI.1136-17.2017]

7 **Bai R**, Guo J, Ye XY, Xie Y, Xie T. Oxidative stress: The core pathogenesis and mechanism of Alzheimer's disease. *Ageing Res Rev* 2022; **77**: 101619 [PMID: 35395415 DOI: 10.1016/j.arr.2022.101619]

8 **Song T**, Song X, Zhu C, Patrick R, Skurla M, Santangelo I, Green M, Harper D, Ren B, Forester BP, Öngür D, Du F. Mitochondrial dysfunction, oxidative stress, neuroinflammation, and metabolic alterations in the progression of Alzheimer's disease: A meta-analysis of in vivo magnetic resonance spectroscopy studies. *Ageing Res Rev* 2021; **72**: 101503 [PMID: 34751136 DOI: 10.1016/j.arr.2021.101503]

9 **Ionescu-Tucker A**, Cotman CW. Emerging roles of oxidative stress in brain aging and Alzheimer's disease. *Neurobiol Aging* 2021; **107**: 86-95 [PMID: 34416493 DOI: 10.1016/j.neurobiolaging.2021.07.014]

10 **Guan L**, Mao Z, Yang S, Wu G, Chen Y, Yin L, Qi Y, Han L, Xu L. Dioscin alleviates Alzheimer's disease through regulating RAGE/NOX4 mediated oxidative stress and inflammation. *Biomed Pharmacother* 2022; **152**: 113248 [PMID: 35691153 DOI: 10.1016/j.biopha.2022.113248]

11 **Abd El-Fatah IM**, Abdelrazek HMA, Ibrahim SM, Abdallah DM, El-Abhar HS. Dimethyl fumarate abridged tauo-/amyloidopathy in a D-Galactose/ovariectomy-induced Alzheimer's-like disease: Modulation of AMPK/SIRT-1, AKT/CREB/BDNF, AKT/GSK-3β, adiponectin/Adipo1R, and NF-κB/IL-1β/ROS trajectories. *Neurochem Int* 2021; **148**: 105082 [PMID: 34052296 DOI: 10.1016/j.neuint.2021.105082]

12 **Ganguly U**, Kaur U, Chakrabarti SS, Sharma P, Agrawal BK, Saso L, Chakrabarti S. Oxidative Stress, Neuroinflammation, and NADPH Oxidase: Implications in the Pathogenesis and Treatment of Alzheimer's Disease. *Oxid Med Cell Longev* 2021; **2021**: 7086512 [PMID: 33953837 DOI: 10.1155/2021/7086512]

13 **Yang H**, Wang G, Liu J, Lin M, Chen J, Fang Y, Li Y, Cai W, Zhan D. LncRNA JPX regulates proliferation and apoptosis of nucleus pulposus cells by targeting the miR-18a-5p/HIF-1α/Hippo-YAP pathway. *Biochem Biophys Res Commun* 2021; **566**: 16-23 [PMID: 34111667 DOI: 10.1016/j.bbrc.2021.05.075]

14 **Zhang L**, Fang Y, Cheng X, Lian YJ, Xu HL. Silencing of Long Noncoding RNA SOX21-AS1 Relieves Neuronal Oxidative Stress Injury in Mice with Alzheimer's Disease by Upregulating FZD3/5 *via* the Wnt Signaling Pathway. *Mol Neurobiol* 2019; **56**: 3522-3537 [PMID: 30143969 DOI: 10.1007/s12035-018-1299-y]

15 **Wang Q**, Ge X, Zhang J, Chen L. Effect of lncRNA WT1-AS regulating WT1 on oxidative stress injury and apoptosis of neurons in Alzheimer's disease *via* inhibition of the miR-375/SIX4 axis. *Aging (Albany NY)* 2020; **12**: 23974-23995 [PMID: 33234729 DOI: 10.18632/aging.104079]

16 **Zhao MY**, Wang GQ, Wang NN, Yu QY, Liu RL, Shi WQ. The long-non-coding RNA NEAT1 is a novel target for Alzheimer's disease progression *via* miR-124/BACE1 axis. *Neurol Res* 2019; **41**: 489-497 [PMID: 31014193 DOI: 10.1080/01616412.2018.1548747]

17 **Chen F**, Han J, Wang D. Identification of key microRNAs and the underlying molecular mechanism in spinal cord ischemia-reperfusion injury in rats. *PeerJ* 2021; **9**: e11454 [PMID: 34123589 DOI: 10.7717/peerj.11454]

18 **Park S**, Lee M, Chun CH, Jin EJ. The lncRNA, Nespas, Is Associated with Osteoarthritis Progression and Serves as a Potential New Prognostic Biomarker. *Cartilage* 2019; **10**: 148-156 [PMID: 28805067 DOI: 10.1177/1947603517725566]

19 **Gao Y**, Zheng X, Chang B, Lin Y, Huang X, Wang W, Ding S, Zhan W, Wang S, Xiao B, Huo L, Yu Y, Chen Y, Gong R, Wu Y, Zhang R, Zhong L, Wang X, Chen Q, Gao S, Jiang Z, Wei D, Kang T. Intercellular transfer of activated STING triggered by RAB22A-mediated non-canonical autophagy promotes antitumor immunity. *Cell Res* 2022; **32**: 1086-1104 [PMID: 36280710 DOI: 10.1038/s41422-022-00731-w]

20 **Kong W**, Li H, Xie L, Cui G, Gu W, Zhang H, Ma W, Zhou Y. LncRNA MCF2L-AS1 aggravates the malignant development of colorectal cancer *via* targeting miR-105-5p/RAB22A axis. *BMC Cancer* 2021; **21**: 1069 [PMID: 34592939 DOI: 10.1186/s12885-021-08668-w]

21 **Yin X**, Chen H, Sun G, Xu Y, Wang L. Circ-C16orf62 Regulates Oxidized low-density Lipoprotein-induced Apoptosis, Inflammation, Oxidative Stress and Cholesterol Accumulation of Macrophages *via* Mediating RAB22A Expression by Targeting miR-377. *Appl Biochem Biotechnol* 2023; **195**: 6586-6606 [PMID: 36892682 DOI: 10.1007/s12010-023-04320-4]

22 **Xie JC**, Ma XY, Liu XH, Yu J, Zhao YC, Tan Y, Liu XY, Zhao YX. Hypoxia increases amyloid-β level in exosomes by enhancing the interaction between CD147 and Hook1. *Am J Transl Res* 2018; **10**: 150-163 [PMID: 29423001]

23 **Bi Z**, Wang Y, Zhang W. A comprehensive review of tanshinone IIA and its derivatives in fibrosis treatment. *Biomed Pharmacother* 2021; **137**: 111404 [PMID: 33761617 DOI: 10.1016/j.biopha.2021.111404]

24 **Ansari MA**, Khan FB, Safdari HA, Almatroudi A, Alzohairy MA, Safdari M, Amirizadeh M, Rehman S, Equbal MJ, Hoque M. Prospective therapeutic potential of Tanshinone IIA: An updated overview. *Pharmacol Res* 2021; **164**: 105364 [PMID: 33285229 DOI: 10.1016/j.phrs.2020.105364]

25 **Ba Z**, Shi S, Huang N, Li Y, Huang J, You C, Yang X, Liu D, Yu C, He Y, Luo Y. Mesenchymal stem cells after the proprocessing of tanshinone IIA attenuate cognitive deficits and oxidative stress injury in an amyloid β-peptide (25-35)-induced rodent model of Alzheimer's disease. *Neuroreport* 2022; **33**: 61-71 [PMID: 34954772 DOI: 10.1097/WNR.0000000000001755]

26 **Ding B**, Lin C, Liu Q, He Y, Ruganzu JB, Jin H, Peng X, Ji S, Ma Y, Yang W. Tanshinone IIA attenuates neuroinflammation *via* inhibiting RAGE/NF-κB signaling pathway in vivo and in vitro. *J Neuroinflammation* 2020; **17**: 302 [PMID: 33054814 DOI: 10.1186/s12974-020-01981-4]

27 **Tao X**, Zhang R, Wang L, Li X, Gong W. Luteolin and Exercise Combination Therapy Ameliorates Amyloid-β1-42 Oligomers-Induced Cognitive Impairment in AD Mice by Mediating Neuroinflammation and Autophagy. *J Alzheimers Dis* 2023; **92**: 195-208 [PMID: 36710678 DOI: 10.3233/JAD-220904]

28 **Ji Q**, Wang X, Cai J, Du X, Sun H, Zhang N. MiR-22-3p Regulates Amyloid β Deposit in Mice Model of Alzheimer's Disease by Targeting Mitogen-activated Protein Kinase 14. *Curr Neurovasc Res* 2019; **16**: 473-480 [PMID: 31713484 DOI: 10.2174/1567202616666191111124516]

29 **Chanda K**, Jana NR, Mukhopadhyay D. Long non-coding RNA MALAT1 protects against Aβ(1-42) induced toxicity by regulating the

expression of receptor tyrosine kinase EPHA2 *via* quenching miR-200a/26a/26b in Alzheimer's disease. *Life Sci* 2022; **302**: 120652 [PMID: 35598655 DOI: 10.1016/j.lfs.2022.120652]

30 **Varesi A**, Carrara A, Pires VG, Floris V, Pierella E, Savioli G, Prasad S, Esposito C, Ricevuti G, Chirumbolo S, Pascale A. Blood-Based Biomarkers for Alzheimer's Disease Diagnosis and Progression: An Overview. *Cells* 2022; **11** [PMID: 35456047 DOI: 10.3390/cells11081367]

31 **Dong LX**, Zhang YY, Bao HL, Liu Y, Zhang GW, An FM. LncRNA NEAT1 promotes Alzheimer's disease by down regulating micro-27a-3p. *Am J Transl Res* 2021; **13**: 8885-8896 [PMID: 34540002]

32 **Peng X**, Chen L, Wang Z, He Y, Ruganzu JB, Guo H, Zhang X, Ji S, Zheng L, Yang W. Tanshinone IIA regulates glycogen synthase kinase-3 β-related signaling pathway and ameliorates memory impairment in APP/PS1 transgenic mice. *Eur J Pharmacol* 2022; **918**: 174772 [PMID: 35090935 DOI: 10.1016/j.ejphar.2022.174772]

33 **Li K**, Wang Z. lncRNA NEAT1: Key player in neurodegenerative diseases. *Ageing Res Rev* 2023; **86**: 101878 [PMID: 36738893 DOI: 10.1016/j.arr.2023.101878]

34 **Nan A**, Zhou X, Chen L, Liu M, Zhang N, Zhang L, Luo Y, Liu Z, Dai L, Jiang Y. A transcribed ultraconserved noncoding RNA, Uc.173, is a key molecule for the inhibition of lead-induced neuronal apoptosis. *Oncotarget* 2016; **7**: 112-124 [PMID: 26683706 DOI: 10.18632/oncotarget.6590]

35 **Hu Q**, Zhang W, Wu Z, Tian X, Xiang J, Li L, Li Z, Peng X, Wei S, Ma X, Zhao Y. Baicalin and the liver-gut system: Pharmacological bases explaining its therapeutic effects. *Pharmacol Res* 2021; **165**: 105444 [PMID: 33493657 DOI: 10.1016/j.phrs.2021.105444]

36 **Mohany M**, Ahmed MM, Al-Rejaie SS. The Role of NF-κB and Bax/Bcl-2/Caspase-3 Signaling Pathways in the Protective Effects of Sacubitril/Valsartan (Entresto) against HFD/STZ-Induced Diabetic Kidney Disease. *Biomedicines* 2022; **10** [PMID: 36359384 DOI: 10.3390/biomedicines10112863]

Published by **Baishideng Publishing Group Inc**
7041 Koll Center Parkway, Suite 160, Pleasanton, CA 94566, USA
Telephone: +1-925-3991568
E-mail: office@baishideng.com
Help Desk: https://www.f6publishing.com/helpdesk
https://www.wjgnet.com